Advanced DNA Detection *via* Multispectral Plasmonic Metasurfaces

Valentina Di Meo[1†], Massimo Moccia[2†], Gennaro Sanità[1,3†], Alessio Crescitelli[1], Annalisa Lamberti[3], Vincenzo Galdi[2], Ivo Rendina[1*] and Emanuela Esposito[1*]

[1] *Institute of Applied Sciences and Intelligent Systems Unit of Naples, National Research Council, Naples, Italy,* [2] *Fields and Waves Laboratory, Department of Engineering, University of Sannio, Benevento, Italy,* [3] *Department of Molecular Medicine and Medical Biotechnology, University of Naples Federico II, Naples, Italy*

We propose and demonstrate a sensing platform based on plasmonic metasurfaces for the detection of very low concentrations of deoxyribo-nucleic acid (DNA) fragments. The platform relies on surface-enhanced infrared absorption spectroscopy, implemented *via* a multispectral metasurface. Specifically, different regions ("pixels") are engineered so as to separately cover the medium-infrared range of the electromagnetic spectrum extending from the functional-groups to the fingerprint region of a single analyte. In conjunction with a suitable bio-functionalization, this enables univocal and label-free recognition of specific molecules. For experimental validation, we fabricate a large-area gold metasurface on a silicon chip, and functionalize it with a recognition layer of peptide nucleic acid (PNA). Our experimental results indicate the possibility to detect complementary DNA fragments in concentrations as low as 50 fM, i.e., well below the value attained by standard methods, with additional advantages in terms of processing time, versatility and ease of implementation/operation.

Keywords: plasmonic metasurface, localized surface plasmon resonances, surface enhanced infrared absorption spectroscopy, DNA biosensor, multiwavelength detection

INTRODUCTION

For the early-stage diagnostic and therapy of genetic diseases, a precise identification of deoxyribo-nucleic acid (DNA) specific sequences is of paramount importance (Dwivedi et al., 2017). Such specificity in DNA sequences detection is also essential in applications requiring viral and bacterial investigation (López et al., 2003). Currently, standard methods (such as polymerase chain reaction, PCR technique) for DNA laboratory analysis are based on DNA amplification, which requires proper experimental design and control to achieve satisfactory sensitivities (Yang and Rothman, 2004). These methods, however, are time- and reagent-consuming, with a limit of detection (LOD) restricted to few nM (Liu et al., 2014; Fakih et al., 2017; Zhang et al., 2019). Therefore, they are not suited for wide-scale DNA testing, which requires instead high sensitivities, as well as small, fast and easy-to-use devices.

Within this framework, infrared (IR) spectroscopy constitutes a potentially attractive candidate, since it allows the univocal and label-free acquisition of direct information on molecules and their functional groups. In essence, IR radiation with wavenumbers within the range $10{,}000–100\ \text{cm}^{-1}$ is absorbed by organic molecules, and then converted into variations of their rotational energy.

In particular, due to the possibility to perform high-speed and standard investigations of several compounds, Fourier-transform IR (FTIR) spectroscopy is one of the most employed analysis tools for a wide range of scenarios of both academic and industrial interest (Stuart, 2004; Griffiths et al., 2007). The spectral range of greatest interest (4,000–400 cm^{-1}) includes the so-called regions of "functional groups" (4,000–1,300 cm^{-1}) and "fingerprint" (1,300–900 cm^{-1}) (Chalmers and Griffiths, 2002). If there is no absorption in the former region, functional groups are absent in the analyzed molecule, whereas the bands appearing within the fingerprint region identify univocal features of the target analyte. However, as predicted by the Beer-Lambert law, the absorption signals become prohibitively weak in the presence of monolayers with minute amounts of analyte (and hence small IR absorption cross-section), which severely curtails the sensitivity of this technique (Amenabar et al., 2013). To overcome this limitation, it is of paramount importance to strongly enhance the light-matter interaction at molecular sites. In surface-enhanced IR absorption (SEIRA) spectroscopy (Le et al., 2008; Adato et al., 2015; Neubrech et al., 2017), this is attained by means of artificial materials such as plasmonic metasurfaces, i.e., 2-D arrays of sub-wavelength metallic inclusions (nanoantennas) (Chen et al., 2016). The functionalization of the metasurfaces is required to specifically capture the target analyte, while an accurate design of the nanoantennas is indispensable to support localized surface plasmon resonances with strong field enhancement (Neubrech et al., 2008; Adato et al., 2011; Di Meo et al., 2019). The optimal sensing conditions for SEIRA occur when the resonance spectrum matches the vibrational signature of the target molecule, so that it is modulated by the absorption phenomenon, thereby allowing its recognition (Adato et al., 2015; Neubrech et al., 2017). It is therefore essential to precisely tune the plasmonic resonances within the spectral range of interest, which can be attained by suitably dimensioning the nanoantenna geometrical parameters (shape, size, thickness and periodicity) (Novotny, 2007). From the fabrication viewpoint, this can be implemented with high spatial reproducibility (Aksu et al., 2010), and the SEIRA sensitivity can be optimized to detect a variety of chemical and biological analytes (Adato and Altug, 2013; Di Meo et al., 2020).

In this study, we report a label-free and real-time detection of DNA fragments by means of SEIRA spectroscopy based on multispectral plasmonic metasurfaces. The proposed device is a large-area (several mm^2) metasurface organized in "pixels," consisting of different spatial regions engineered so as to work within separate IR spectral regions of interest (spanning from the fingerprint region to the region of the functional groups). Pixels are constituted by 2D arrays of cross-shaped gold nanoantennas, realized on a silicon substrate by means of electron beam lithography (EBL), which ensures a reproducible fabrication of homogeneous and robust devices (Di Meo et al., 2019). The plasmonic response of each array (arising from both the collective and individual response of the nanoantennas) generates enhancement factors up to 10^6. Furthermore, the symmetric shape of the nanoantennas minimizes the sensitivity with respect to the polarization of the impinging radiation and to the random orientation of the target analyte dipole moment.

In order to detect DNA fragments, we exploit a peptide nucleic acid (PNA) as a recognition layer, since its IR spectrum is different from that of DNA. Moreover, due to its properties, PNA exhibits a higher affinity and specificity binding capabilities to complementary nucleic acids with respect to traditional oligonucleotides (Wittung et al., 1994), even higher than the corresponding ssDNA sequence (Wang, 1998). For these reasons, PNA is one of the most widely employed tools for the development of innovative biosensors. We are able to detect DNA fragments at a concentration as low as 50 fM, therefore much lower than traditional methods, in a label-free and real-time modality. These results demonstrate the very promising potential of the proposed approach, which is non-destructive, fast, cost-effective, and based on miniaturized devices. As a more general outcome, our study indicates that the knowledge of the IR absorption properties of a given molecule can be effectively used to detect its presence, providing the molecular fingerprint at extremely low concentrations.

MATERIALS AND METHODS

Modeling and Design

The plasmonic metasurfaces in our study are modeled and designed by means of finite-element numerical simulations carried out via the commercial software package Ansys HFSS electromagnetics suite 16.2[1]. Referring to **Figures 1A,B** for a schematic illustration, we assume a silicon substrate [with refractive index taken from (Chandler-Horowitz and Amirtharaj, 2005)] overlayed with a 2-D periodic arrangement of cross-shaped gold nanoantennas of thickness $t = 50$nm, period P, arm-length L, arm-width W, and electrical conductivity $\sigma = 15 \times 10^6$ S/m (Laman and Grischkowsky, 2008), with an exterior air region.

The structure, assumed of infinite extent in the transverse plane, is modeled considering a single period (unit cell, **Figure 1A**), under plane-wave illumination normally impinging from the air region. Accordingly, master/slave periodicity conditions are enforced at the lateral walls, whereas a Floquet-type port and a perfectly matched layer are assumed as terminations of air region (of thickness 10 μm) and substrate (of thickness 5 μm), respectively. The computational domain is finally discretized via standard meshing (resulting in ∼160,000 elements) and the problem is numerically solved by means of the standard iterative solver with default converge conditions.

Based on an extensive set of parametric studies, we identify the resonance regimes and investigate their dependence on the geometrical parameters; this enables the tuning of the resonant lineshapes within the spectral region of interest. **Figure 1C** shows the numerically simulated reflectance spectra pertaining to the four design selected (with geometrical and resonance details summarized in **Table 1**). We also observe some abrupt changes of slopes at specific wavenumbers, which are due to the well-known Rayleigh-Wood anomalies for the transmitted field (Maystre, 2012). A representative resonant-field distribution is shown in
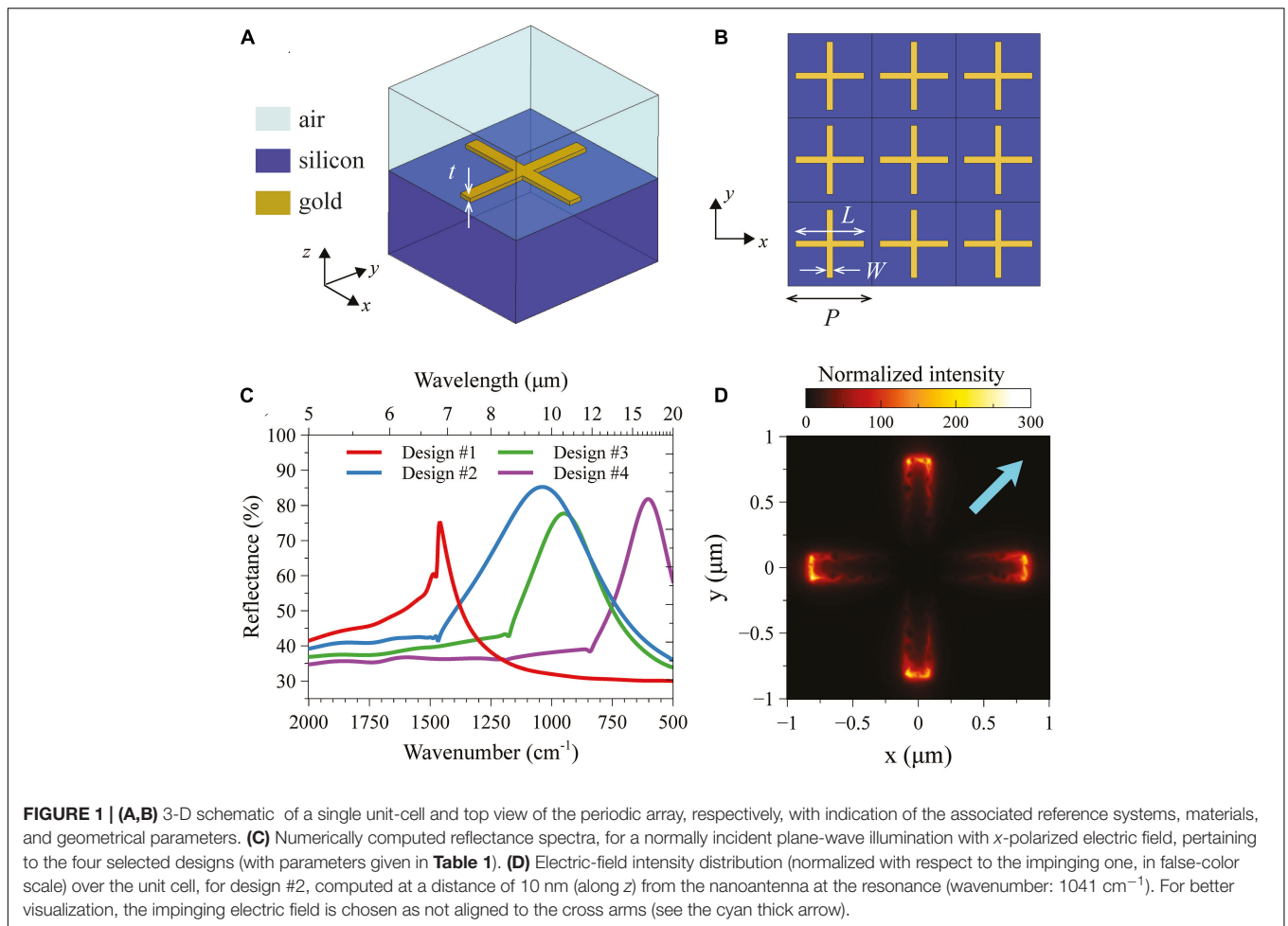
---

[1]https://www.ansys.com/products/electronics/ansys-hfss

FIGURE 1 | (A,B) 3-D schematic of a single unit-cell and top view of the periodic array, respectively, with indication of the associated reference systems, materials, and geometrical parameters. **(C)** Numerically computed reflectance spectra, for a normally incident plane-wave illumination with *x*-polarized electric field, pertaining to the four selected designs (with parameters given in **Table 1**). **(D)** Electric-field intensity distribution (normalized with respect to the impinging one, in false-color scale) over the unit cell, for design #2, computed at a distance of 10 nm (along *z*) from the nanoantenna at the resonance (wavenumber: 1041 cm^{-1}). For better visualization, the impinging electric field is chosen as not aligned to the cross arms (see the cyan thick arrow).

TABLE 1 | Nominal geometrical parameters for the four designs in **Figure 1C**, with indication of the corresponding (simulated) resonance wavenumbers.

Pixel	L (µm)	W (µm)	P (µm)	ν_{res}^{sim} (cm^{-1})
#1	1.1	0.2	2.0	1,461
#2	1.7	0.2	2.0	1,041
#3	2.0	0.2	2.5	947
#4	3.0	0.2	3.5	604

Figure 1D as a normalized intensity map (in false-color scale) over a single unit cell. As typical for plasmonic nanoantennas, we observe that the field is strongly enhanced (up to a factor ∼300) at the arm tips, yielding very pronounced hotspots.

Fabrication Methods

The multispectral metasurfaces are fabricated on a 1 cm^2 silicon wafer die, with the coverage area spanning over 1.5 mm × 1.5 mm. As schematically illustrated in **Figure 2A**, the metasurface comprises four different pixels, according to the designs in **Figure 1C** and **Table 1**. In particular, the resonance wavenumbers span the range 600–1,500 cm^{-1}, in order to include the fingerprint region. Each pixel is identified by its coordinates on the die (with respect to a fixed Cartesian system), and covers an area of 500 µm × 500 µm, which is well matched with the typical 100 µm × 100 µm beam-width of the FTIR spectrometer. The fabrication relies on the EBL technique, whereby each nanoantenna is first patterned in electron resist, and the design is then transferred into a 50 nm gold film *via* a lift-off process (Crescitelli et al., 2012). **Figure 2B** shows a scanning electron microscope (SEM) image of a representative pixel, with a magnified view of a single nanoantenna. The standard method utilized guarantees a very high reliability level, and the fabricated devices are reusable. All the details on the fabrication process and related data are reported in the supplementary information of (Di Meo et al., 2019), and are not repeated here.

Functionalization Procedure

To detect the capture of DNA on the metasurface pixels, we use a single-stranded PNA (ssPNA) as recognition layer that supports the DNA base pairing mechanisms. Indeed, PNA emulates structural DNA by substituting its typical ribose phosphate backbone with N-(2-aminoethyl) glycine linkage. As shown in **Figure 3A**, methylene carbonyl linkers bind the nitrogenous bases of PNA to the polyamide structure (Nielsen et al., 1991; Egholm et al., 1992).
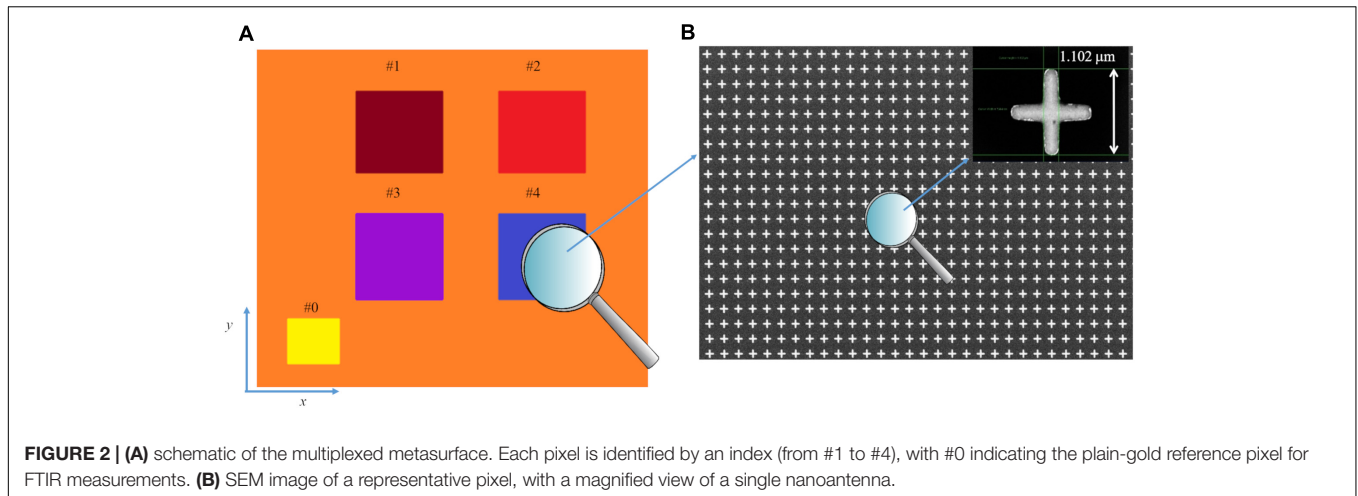
FIGURE 2 | (A) schematic of the multiplexed metasurface. Each pixel is identified by an index (from #1 to #4), with #0 indicating the plain-gold reference pixel for FTIR measurements. **(B)** SEM image of a representative pixel, with a magnified view of a single nanoantenna.
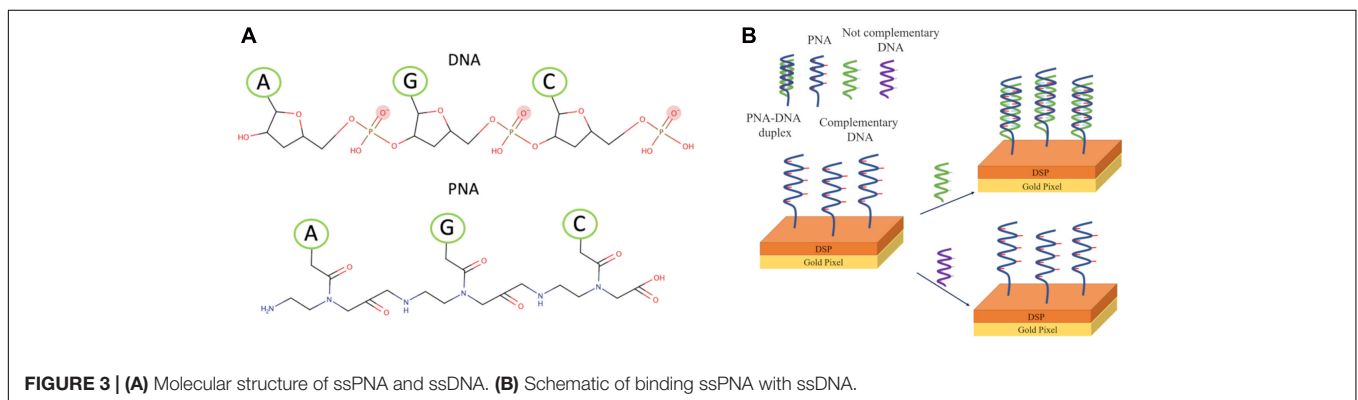

FIGURE 3 | (A) Molecular structure of ssPNA and ssDNA. **(B)** Schematic of binding ssPNA with ssDNA.
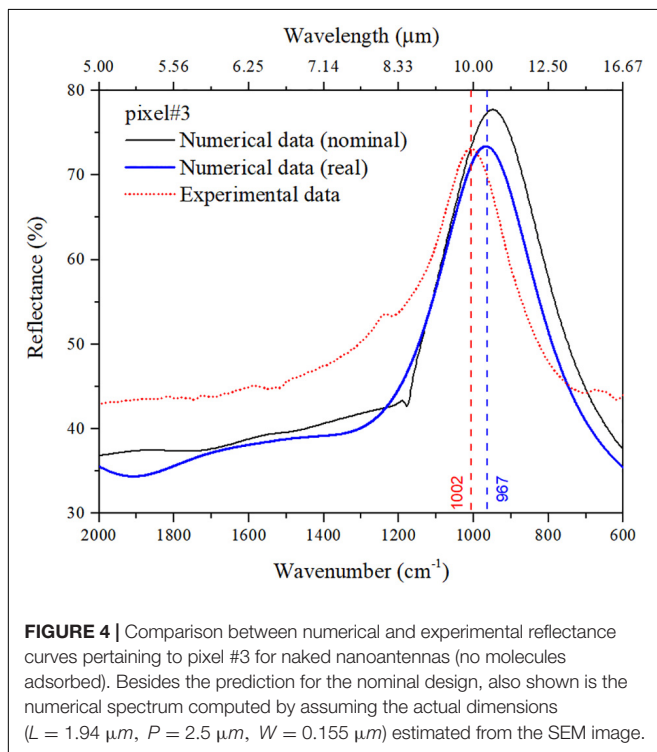

FIGURE 4 | Comparison between numerical and experimental reflectance curves pertaining to pixel #3 for naked nanoantennas (no molecules adsorbed). Besides the prediction for the nominal design, also shown is the numerical spectrum computed by assuming the actual dimensions ($L = 1.94 \, \mu m$, $P = 2.5 \, \mu m$, $W = 0.155 \, \mu m$) estimated from the SEM image.

All pixels are bio-functionalized with RAS-PNA-NH_2 by using dithiobis (succinimidyl propionate) (DSP) as linker. In particular, the pixels are washed with dimethyl sulfoxide (DMSO), isopropyl alcohol, and bi-distilled water for 5′ under stirring. After drying by N_2 flux, the gold surface is incubated with DSP 4 mg/ml in DMSO for 60′ at room temperature. After extensive washing with DMSO, bi-distilled water and phosphate buffered saline (PBS) solution 1×, the surface is incubated with RAS-PNA-NH_2 (molecular weight, MW = 3,714 Da) 80 μM in PBS over night at 4°C. Next, after extensive washing with PBS 1× and bi-distilled water, the pixels are dried by N_2 fluxed, and incubated with complementary DNA (cDNA) (MW = 3,572 Da) at 50 fM, 500 fM and 5 pM, or with not complementary DNA (ncDNA) (MW = 3,748 Da) at 50 pM in PBS 1× for 6 h at 4°C. After washing with PBS 1× and bi-distilled water to remove the unbounded DNA, the pixels are dried with N_2 flux. Binding measurements are carried out *via* the procedure described above. A scheme of the binding process is shown in **Figure 3B**.

IR Measurements

The reflectance spectra are acquired by means of a Thermo-Nicholet NEXUS Continuum XL (Thermo Scientific, Waltham, MA, United States) spectrometer equipped with a nitrogen cooled mercury cadmium telluride detector and
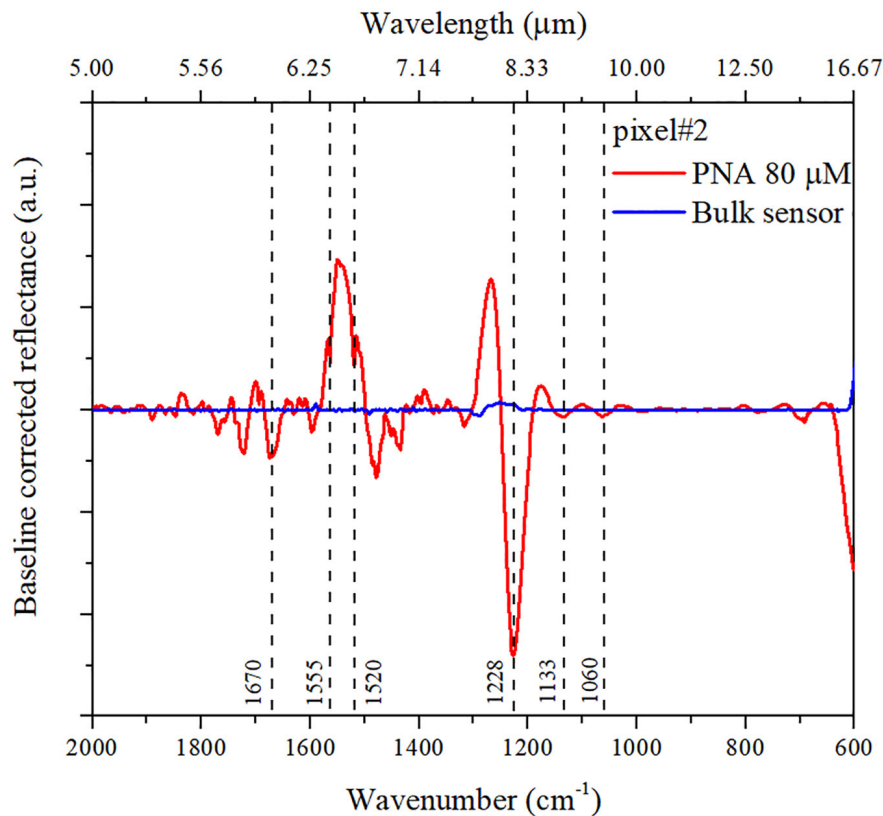
FIGURE 5 | SEIRA baseline-corrected reflectance spectra pertaining to pixel #2. The blue curve pertains to the pixel without functionalization (i.e., naked nanoantennas); the red curve pertains to nanoantennas with PNA molecules linked, with the detected molecular vibrations as described into the text.

a focal-plane-array detector. Knife-edge apertures are set to delimit a measurement area of $100 \times 100 \ \mu m^2$. Measurements are carried out at room temperature on dried samples, by collecting 200 scans with a resolution of $4 \ cm^{-1}$ within the range $4,000–600 \ cm^{-1}$. All acquired spectra are normalized with respect to a background that is collected on a plain gold film deposited on the same substrate of the multispectral metasurface (pixel #0 in **Figure 2A**).

RESULTS AND DISCUSSION

Figure 4 shows a comparison between simulated and measured reflectance spectra of a representative pixel. In this particular example, pixel #3 exhibits a plasmonic resonance at a nominal wavenumber of $947 \ cm^{-1}$ with $\sim$75% reflectance. As can be observed, the position of the experimental resonance peak is in fair agreement with the numerical prediction for the nominal design (see **Table 1**). The discrepancies are mostly attributable to fabrication tolerances, and indeed the agreement improves if the actual nanoantenna dimensions estimated from the SEM images are considered in the simulations (see blue curve). Overall, our design procedure of the metasurface pixels turns out to provide sufficient accuracy for tuning the desired spectral characteristics.

As previously mentioned, the specific detection of DNA sequences is fundamental for the diagnostic and treatment of genetic-related diseases (Yang et al., 1997; Dwivedi et al., 2017). To detect the capture of DNA on the metasurface pixels, we exploit PNA as a recognition layer that supports the DNA base pairing mechanisms (Wang, 1998). The reference analytical characterization used in our experiment, based on the FTIR analysis of solid samples of *RAS*-PNA-NH2 and complementary DNA ($1.68 \ \mu M$ each), is provided in the **Supplementary Material** (**Supplementary Figure 1**). Precisely by virtue of the chemical differences between DNA and PNA, we are able to recognize the DNA binding on our nanoantennas through the signature of the vibrational band of the sugar-phosphate backbone ($1,000–1,300 \ cm^{-1}$) (more specifically, *via* the asymmetric stretching vibration of PO_4^- group). The gold nanoantennas are functionalized with a *RAS*-PNA recognition layer, and the FTIR spectra are examined before and after the PNA binding on their surface, and once again after the binding with the DNA. The absolute amount of PNA molecules linked on the whole chip area of $1 \ cm^2$ is estimated to be 1.60 nmol (a droplet of $20 \ \mu L$ at a concentration of $80 \ \mu M$ is adsorbed). Considering an effective area coverage exposed to the light of $100 \times 100 \ \mu m^2$, we are able to detect in a single measurement an absolute amount of 160 fmol of PNA. **Figure 5** shows the SEIRA
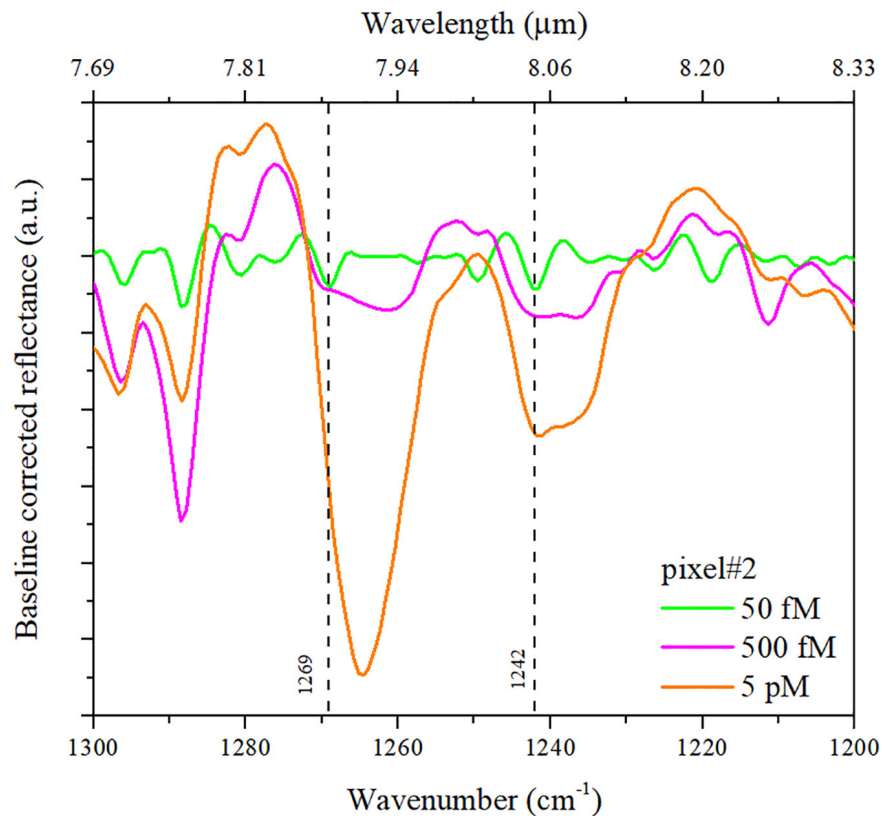
FIGURE 6 | SEIRA baseline-corrected reflectance spectra pertaining to pixel #2 at different concentrations of cDNA: 50 fM (green curve), 500 fM (purple), and 5 pM (orange).

baseline-corrected reflectance spectra pertaining to pixel #2 (red curve) after the binding of PNA molecules, and the FTIR baseline-corrected reflectance spectra of the same pixel without functionalization (blue curve) as a negative control. Pixel #2 is characterized by a naked resonance nominally centered at $1,041 \text{ cm}^{-1}$.

The SEIRA spectra pertaining to pixel #2 show the signature of PNA, as deduced from a comparison with the spectrum pertaining to a solid sample of the same PNA molecules utilized in the experiment (see **Supplementary Figure 1**). In particular, the bending vibrations [δ(C-H) and δ(N-H)] and in-plane vibration mode (of C-C and C = N) (Wang et al., 2001; Yamada et al., 2004) of adenine and cytosine nitrogenous bases appear around $1,550 \text{ cm}^{-1}$. Other vibrations that appear in the same region are related to the amide group: Amide I around $1,650 \text{ cm}^{-1}$ (C = O stretch) and Amide II at $1,540 \text{ cm}^{-1}$ (NH deformation). These frequencies are difficult to identify because they are mixed with the nucleic base absorptions and exhibit very low intensity (Mateo-Martí et al., 2005). **Figure 6** shows the SEIRA baseline-corrected reflectance spectra pertaining to pixel #2 after the binding of the PNA recognition layer with the complementary DNA (cDNA) at different concentrations (from 50 fM to 5 pM).

Once the bond occurs between the PNA and DNA, the sugar-phosphate conformation is present. The SEIRA

spectra in **Figure 6** exhibit the vibrational band of the sugar-phosphate backbone $(1,000–1,300 \text{ cm}^{-1})$ (Banyay et al., 2003) (more specifically, the asymmetric stretching vibration of PO_4^-). The antisymmetric PO_2^- stretching band is a characteristic marker for nucleic acid backbone conformation, independent of nitrogenous bases vibrations and sugar pucker. As the concentration is reduced to 50 fM, the intensity of the bands is reduced, but the signature remains well visible at 1,269 and $1,242 \text{ cm}^{-1}$. However, since these bands are found within the fingerprint region, it is not always easy to assign them. In addition, the vibrational characteristics of the chemical groups of nucleic acid (especially PO_2^-) also depend on the DNA composition (Mello and Vidal, 2012).

Pixel #1 is characterized by a naked resonance nominally centered at $1,461 \text{ cm}^{-1}$. After the binding with the correlated DNA, it exhibits SEIRA vibrational bands, corresponding to base–sugar vibrations, within the region $1,394–1,311 \text{ cm}^{-1}$. This region is sensitive to glycosidic bond rotation, backbone conformation and sugar pucker (Peng et al., 2011). The SEIRA baseline-corrected reflectance spectra pertaining to pixel #1 are shown in **Figure 7**.

To sum up, based on the reference IR analysis carried out on the DNA sample in solid form (**Supplementary Figure 1**), it is possible to associate all the peaks highlighted through
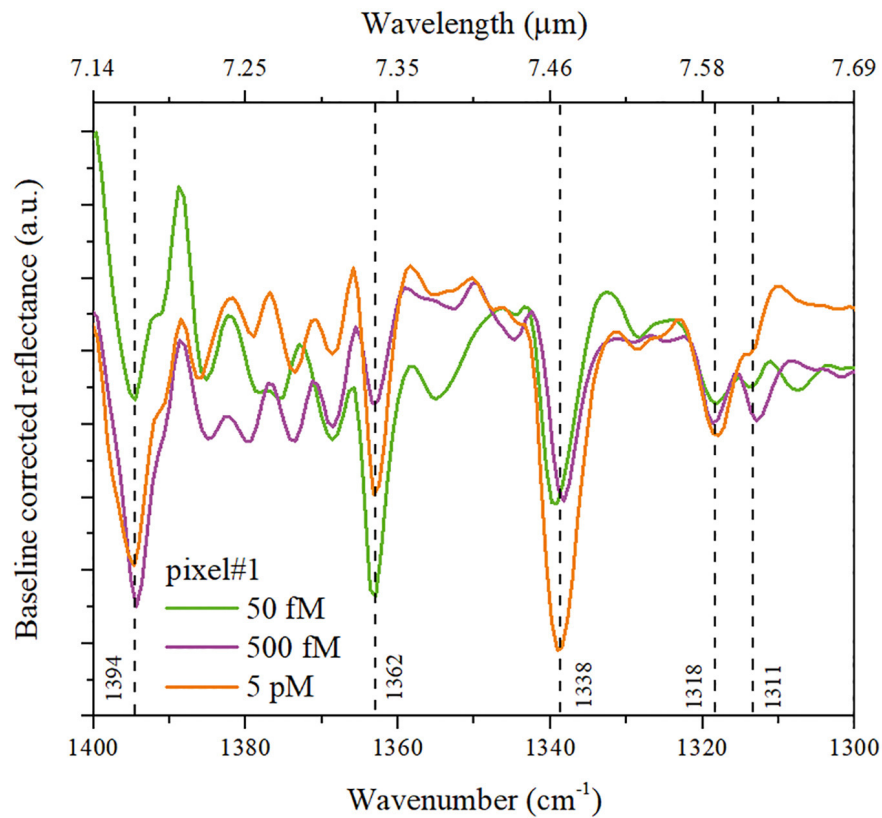
FIGURE 7 | SEIRA baseline-corrected reflectance spectra pertaining to pixel #1 at different concentrations of cDNA: 50 fM (green curve), 500 fM (purple), and 5 pM (orange).

the SEIRA effect to the corresponding vibrational bands of the molecule.

As previously mentioned, in order to attain a manageable vibrational signal, it is crucial to precisely tune the nanoantenna resonances within the different vibration bands. The sensitivity of resonant SEIRA effects can be quantified in terms of the enhancement factor (EF) (Neubrech et al., 2017).

$$EF = \frac{\Delta R}{\Delta R_0} \cdot \frac{A_0}{A_{SEIRA}} \qquad (1)$$

with ΔR denoting the reflectance difference (at the vibrational signature) in the absence and presence of the molecules, and ΔR_0 the reflectance difference with respect to a flat gold layer with same thickness as the nanoantennas (pixel #0 in **Figure 2A**). Moreover, A_0 indicates the effective area of the nanoantennas illuminated (100 μm × 100 μm, in our case), and A_{SEIRA} the effective area of the nanoantennas on which the field is localized. As well known (Neubrech et al., 2008; Adato et al., 2011; Di Meo et al., 2019, 2020), and also observed in **Figure 1D**, the resonant field tends to be mainly localized at the tips of the nanoantenna arms. As detailed in the **Supplementary Material**, we estimate EF values of 7×10^6 for pixel #2, and 2.3×10^6 for pixel #1, which turn out to be among the largest values reported in the literature (typically ranging from 10^3 to 10^5) (De Tommasi et al., 2021), thereby confirming the attractive

performance of our devices and the very promising potential of the approach.

The minimum concentration of correlated DNA fragments detected in our experiment is 50 fM, which is well below the value (0.87 nM) determined by standard and innovative methods (Liu et al., 2014; Fakih et al., 2017; Zhou et al., 2018, 2019a,b; Zhang et al., 2019). The absolute amount of DNA molecules detected for this last concentration is 1 amol spread on a die area of 1 cm², corresponding to an actual amount on the detection area of 100 × 100 μm² in the zepto molar range. In a parallel control experiment, we also verified the specificity of the molecular recognition by exposing the sensor to a non-complementary DNA (ncDNA) at 50 pM. As shown in the **Supplementary Material**, in this case, we do not observe any difference in the reflectance spectra of our device before and after the linking procedure with the active layer of PNA (see **Supplementary Figure 2**), thereby confirming the failure of the binding procedure, and hence the selectivity of the proposed platform.

As shown in the **Supplementary Material**, the dynamic curve of our sensor exhibits a linear behavior, thereby suggesting the possibility to further lower the LOD (see **Supplementary Figure 3**). Although the range we have explored does not represent the full working range, we will plan further experiments close to the noise level in order to estimate the ultimate LOD.

It is worth emphasizing that, besides the capability to detect extremely low concentrations of analyte, our proposed sensor based on multispectral metasurfaces compares favorably with traditional methods based on radioactive compounds (Wei et al., 2010), since it does not require long response times, large amount of reagents, disposal, pretreatment procedures, and expensive instrumentation.

CONCLUSION

In this study, we have demonstrated a multispectral plasmonic metasurface sensor for the multiwavelength detection of ssDNA at very low concentration based on SEIRA spectroscopy. Unlike many traditional methods (based on radioactive compounds), our technology enables a label-free and real time detection, thus providing inherent advantages, including cost effectiveness. We have verified the DNA detection capability of our sensing platform using PNA molecules as a recognition layer that supports the DNA base pairing mechanisms, thereby ensuring selectivity and specificity. We have recognized the molecular fingerprint of the DNA through the identification of the specific vibrational bands in the SEIRA spectra. The measured LOD is 50 fM, which corresponds to an absolute amount of 1 amol of DNA molecules over the whole die area, which is significantly lower than the values characterizing both traditional and innovative approaches proposed so far. Overall, the obtained results indicate promising perspectives for the technology underpinning our biosensor. It can be extended to the detection of viruses and other pathogens by functionalizing the sensing metasurface with suitable probes—like antibodies—able to specifically recognize target antigens expressed on the pathogens surface.

DATA AVAILABILITY STATEMENT

The original contributions presented in the study are included in the article/**Supplementary Material**, further inquiries can be directed to the corresponding author/s.

AUTHOR CONTRIBUTIONS

VDM manufactured the devices and analyzed the data. MM designed and simulated the devices. GS functionalized the devices and performed the trials using FTIR spectrometer. AC contributed to the manufacturing. AL supervised the functionalization and trials. VG supervised the design and modeling, and wrote the manuscript. IR supervised the device realization. EE conceived the idea, led the investigation, analyzed the data, and wrote the manuscript. All authors reviewed the manuscript.

FUNDING

SUPPLEMENTARY MATERIAL

The Supplementary Material for this article can be found online at: https://www.frontiersin.org/articles/10.3389/fbioe. 2021.666121/full#supplementary-material

REFERENCES

Adato, R., Aksu, S., and Altug, H. (2015). Engineering mid-infrared nanoantennas for surface enhanced infrared absorption spectroscopy. *Mater. Today* 18, 436–446. doi: 10.1016/j.mattod.2015.03.001

Adato, R., and Altug, H. (2013). In-situ ultra-sensitive infrared absorption spectroscopy of biomolecule interactions in real time with plasmonic nanoantennas. *Nat. Commun.* 4:2154. doi: 10.1038/ncomms3154

Adato, R., Yanik, A. A., and Altug, H. (2011). On chip plasmonic monopole nano-antennas and circuits. *Nano Lett.* 11, 5219–5226. doi: 10.1021/nl202528h

Aksu, S., Yanik, A. A., Adato, R., Artar, A., Huang, M., and Altug, H. (2010). High-throughput nanofabrication of infrared plasmonic nanoantenna arrays for vibrational nanospectroscopy. *Nano Lett.* 10, 2511–2518. doi: 10.1021/nl101042a

Amenabar, I., Poly, S., Nuansing, W., Hubrich, E. H., Govyadinov, A. A., Huth, F., et al. (2013). Structural analysis and mapping of individual protein complexes by infrared nanospectroscopy. *Nat. Commun.* 4:2890. doi: 10.1038/ncomms3890

Banyay, M., Sarkar, M., and Gräslund, A. (2003). A library of IR bands of nucleic acids in solution. *Biophys. Chem.* 104, 477–488. doi: 10.1016/S0301-4622(03)00035-38

Chalmers, J. M., and Griffiths, P. R. (2002). *Handbook of Vibrational Spectroscopy*. New York, NY: Wiley.

Chandler-Horowitz, D., and Amirtharaj, P. M. (2005). High-accuracy, midinfrared (450cm-1⩽ω⩽4000cm-1) refractive index values of silicon. *J. Appl. Phys.* 97:123526. doi: 10.1063/1.1923612

Chen, H.-T., Taylor, A. J., and Yu, N. (2016). A review of metasurfaces: physics and applications. *Rep. Prog. Phys.* 79, 1–40. doi: 10.1088/0034-4885/79/7/076401

Crescitelli, A., Ricciardi, A., Consales, M., Esposito, E., Granata, C., Galdi, V., et al. (2012). Nanostructured metallo-dielectric quasi-crystals: towards photonic-plasmonic resonance engineering. *Adv. Funct. Mater.* 22, 4389–4398. doi: 10.1002/adfm.201200217

De Tommasi, E., Esposito, E., Romano, S., Crescitelli, A., Di Meo, V., Mocella, V., et al. (2021). Frontiers of light manipulation in natural, metallic, and dielectric nanostructures. *Riv. Nuovo Cim* 44, 1–68. doi: 10.1007/s40766-021-00015-w

Di Meo, V., Caporale, A., Crescitelli, A., Janneh, M., Palange, E., De Marcellis, A., et al. (2019). Metasurface based on cross-shaped plasmonic nanoantennas as chemical sensor for surface-enhanced infrared absorption spectroscopy. *Sens. Actuators B Chem.* 286, 600–607. doi: 10.1016/j.snb.2019.02.014

Di Meo, V., Crescitelli, A., Moccia, M., Sandomenico, A., Cusano, A. M., Portaccio, M., et al. (2020). Pixeled metasurface for multiwavelength detection of vitamin D. *Nanophotonics* 9, 3921–3930. doi: 10.1515/nanoph-2020-2103

Dwivedi, S., Purohit, P., Misra, R., Pareek, P., Goel, A., Khattri, S., et al. (2017). Diseases and molecular diagnostics: a step closer to precision medicine. *Indian J. Clin. Biochem.* 32, 374–398. doi: 10.1007/s12291-017-0688-688

Egholm, M., Buchardt, O., Nielsen, P. E., and Berg, R. H. (1992). Peptide nucleic acids (PNA). Oligonucleotide analogs with an achiral peptide backbone. *J. Am. Chem. Soc.* 114, 1895–1897. doi: 10.1021/ja00031a062

Fakih, H. H., Itani, M. M., and Karam, P. (2017). Gold nanoparticles-coated polystyrene beads for the multiplex detection of viral DNA. *Sens. Actuators B Chem.* 250, 446–452. doi: 10.1016/j.snb.2017.04.066

Griffiths, P. R., De Haseth, J. A., and Winefordner, J. D. (2007). *Fourier Transform Infrared Spectrometry*. New York, NY: Wiley.

Laman, N., and Grischkowsky, D. (2008). Terahertz conductivity of thin metal films. *Appl. Phys. Lett.* 93:051105. doi: 10.1063/1.2968308

Le, F., Brandl, D. W., Urzhumov, Y. A., Wang, H., Kundu, J., Halas, N. J., et al. (2008). Metallic nanoparticle arrays: a common substrate for both surface-enhanced Raman scattering and surface-enhanced infrared absorption. *ACS Nano* 2, 707–718. doi: 10.1021/nn800047e

Liu, Z.-C., Zhang, L., Zhang, Y.-M., Liang, R.-P., and Qiu, J.-D. (2014). Exonuclease III-assisted recycling amplification detection of hepatitis B virus DNA by DNA-scaffolded silver nanoclusters probe. *Sens. Actuators B Chem.* 205, 219–226. doi: 10.1016/j.snb.2014.08.079

López, M. M., Bertolini, E., Olmos, A., Caruso, P., Gorris, M. T., Llop, P., et al. (2003). Innovative tools for detection of plant pathogenic viruses and bacteria. *Int. Microbiol.* 6, 233–243. doi: 10.1007/s10123-003-0143-y

Mateo-Martí, E., Briones, C., Román, E., Briand, E., Pradier, C. M., and Martín-Gago, J. A. (2005). Self-assembled monolayers of peptide nucleic acids on gold surfaces: a Spectroscopic Study. *Langmuir* 21, 9510–9517. doi: 10.1021/la050366v

Maystre, D. (2012). "Theory of wood's anomalies," in *Plasmonics: From Basics to Advanced Topics*, eds S. Enoch and N. Bonod (Berlin: Springer Berlin Heidelberg), 39–83. doi: 10.1007/978-3-642-28079-5_2

Mello, M. L. S., and Vidal, B. C. (2012). Changes in the infrared microspectroscopic characteristics of DNA caused by cationic elements, different base richness and single-stranded form. *PLoS One* 7:e43169. doi: 10.1371/journal.pone.0043169

Neubrech, F., Huck, C., Weber, K., Pucci, A., and Giessen, H. (2017). Surface-enhanced infrared spectroscopy using resonant nanoantennas. *Chem. Rev.* 117, 5110–5145. doi: 10.1021/acs.chemrev.6b00743

Neubrech, F., Pucci, A., Cornelius, T. W., Karim, S., García-Etxarri, A., and Aizpurua, J. (2008). Resonant plasmonic and vibrational coupling in a tailored nanoantenna for infrared detection. *Phys. Rev. Lett.* 101:157403. doi: 10.1103/PhysRevLett.101.157403

Nielsen, P. E., Egholm, M., Berg, R. H., and Buchardt, O. (1991). Sequence-selective recognition of DNA by strand displacement with a thymine-substituted polyamide. *Science* 254, 1497–1500. doi: 10.1126/science.1962210

Novotny, L. (2007). Effective wavelength scaling for optical antennas. *Phys. Rev. Lett.* 98:266802. doi: 10.1103/PhysRevLett.98.266802

Peng, C. S., Jones, K. C., and Tokmakoff, A. (2011). Anharmonic vibrational modes of nucleic acid bases revealed by 2D IR spectroscopy. *J. Am. Chem. Soc.* 133, 15650–15660. doi: 10.1021/ja205636h

Stuart, B. H. (2004). *Infrared Spectroscopy: Fundamentals and Applications*. New York, NY: Wiley.

Wang, J. (1998). DNA biosensors based on Peptide Nucleic Acid (PNA) recognition layers. a review. *Biosens. Bioelectron.* 13, 757–762. doi: 10.1016/S0956-5663(98)00039-36

Wang, Z., Liu, D., and Dong, S. (2001). In-situ FTIR study on adsorption and oxidation of native and thermally denatured calf thymus DNA at glassy carbon electrodes. *Biophys. Chem.* 89, 87–94. doi: 10.1016/S0301-4622(00)00217-9

Wei, F., Lillehoj, P. B., and Ho, C.-M. (2010). DNA diagnostics: nanotechnology-enhanced electrochemical detection of nucleic acids. *Pediatr. Res.* 67, 458–468. doi: 10.1203/PDR.0b013e3181d361c3

Wittung, P., Nielsen, P. E., Buchardt, O., Egholm, M., and Norde'n, B. (1994). DNA-like double helix formed by peptide nucleic acid. *Nature* 368, 561–563. doi: 10.1038/368561a0

Yamada, T., Shirasaka, K., Takano, A., and Kawai, M. (2004). Adsorption of cytosine, thymine, guanine and adenine on Cu(110) studied by infrared reflection absorption spectroscopy. *Surf. Sci.* 561, 233–247. doi: 10.1016/j.susc.2004.05.095

Yang, M., McGovern, M. E., and Thompson, M. (1997). Genosensor technology and the detention of interfacial nucleic acid chemistry. *Analytica Chimica Acta* 346, 259–275. doi: 10.1016/S0003-2670(97)90055-90056

Yang, S., and Rothman, R. E. (2004). PCR-based diagnostics for infectious diseases: uses, limitations, and future applications in acute-care settings. *Lancet Infect. Dis.* 4, 337–348. doi: 10.1016/S1473-3099(04)01044-1048

Zhang, K., Huang, W., Huang, Y., Li, H., Wang, K., Zhu, X., et al. (2019). DNA tetrahedron based biosensor for Argonaute2 assay in single cells and human immunodeficiency virus type-1 related ribonuclease H detection in vitro. *Anal. Chem.* 91, 7086–7096. doi: 10.1021/acs.analchem.9b00011

Zhou, H., Hu, D., Yang, C., Chen, C., Ji, J., Chen, M., et al. (2018). Multi-band sensing for dielectric property of chemicals using metamaterial integrated microfluidic sensor. *Sci. Rep.* 8:14801. doi: 10.1038/s41598-018-32827-y

Zhou, H., Yang, C., Hu, D., Dou, S., Hui, X., Zhang, F., et al. (2019a). Integrating a microwave resonator and a microchannel with an immunochromatographic strip for stable and quantitative biodetection. *ACS Appl. Mater. Interfaces* 11, 14630–14639. doi: 10.1021/acsami.9b02087

Zhou, H., Yang, C., Hu, D., Li, D., Hui, X., Zhang, F., et al. (2019b). Terahertz biosensing based on bi-layer metamaterial absorbers toward ultra-high sensitivity and simple fabrication. *Appl. Phys. Lett.* 115:143507. doi: 10.1063/1.5111584